arXiv:1904.04694v1 [physics.space-ph] 9 Apr 2019

FORBUSH DECREASES AND < 2-DAY GCR FLUX NON-RECURRENT VARIATIONS STUDIED WITH LISA PATHFINDER

M. Armano,[1] H. Audley,[2] J. Baird,[3] S. Benella,[4,5] P. Binetruy,[6,*] M. Born,[2]
D. Bortoluzzi,[7] E. Castelli,[8] A. Cavalleri,[9] A. Cesarini,[4] A. M. Cruise,[10] K. Danzmann,[2]
M. de Deus Silva,[1] I. Diepholz,[2] G. Dixon,[10] R. Dolesi,[11] M. Fabi,[4] L. Ferraioli,[12]
V. Ferroni,[11] N. Finetti,[5,13] E. D. Fitzsimons,[14] M. Freschi,[1] L. Gesa,[15] F. Gibert,[11]
D. Giardini,[12] R. Giusteri,[11] C. Grimani,[4,5] J. Grzymisch,[16] I. Harrison,[17] G. Heinzel,[2]
M. Hewitson,[2] D. Hollington,[3] D. Hoyland,[10] M. Hueller,[11] H. Inchauspé,[6] O. Jennrich,[16]
P. Jetzer,[18] N. Karnesis,[2] B. Kaune,[2] N. Korsakova,[19] C. J. Killow,[19] K. Kudela,[20,†]
M. Laurenza,[5,21] J. A. Lobo,[15,‡] I. Lloro,[15] L. Liu,[11] J. P. López-Zaragoza,[15]
R. Maarschalkerweerd,[17] D. Mance,[12] N. Meshksar,[12] V. Martín,[15] L. Martin-Polo,[1]
J. Martino,[6] F. Martin-Porqueras,[1] I. Mateos,[15] P. W. McNamara,[16] J. Mendes,[17]
L. Mendes,[1] M. Nofrarias,[15] S. Paczkowski,[2] M. Perreur-Lloyd,[19] A. Petiteau,[6]
P. Pivato,[11] E. Plagnol,[6] J. Ramos-Castro,[22] J. Reiche,[2] D. I. Robertson,[19] F. Rivas,[15]
G. Russano,[11] J. Slutsky,[23] C. F. Sopuerta,[15] T. Sumner,[3] D. Telloni,[5,24] D. Texier,[1]
J. I. Thorpe,[23] D. Vetrugno,[11] M. Villani,[4,5] S. Vitale,[11] G. Wanner,[2] H. Ward,[19] P. Wass,[3]
W. J. Weber,[11] L. Wissel,[2] A. Wittchen,[2] and P. Zweifel[12]

[1] *European Space Astronomy Centre, European Space Agency*

Villanueva de la Cañada
28692 Madrid, Spain

[2] *Albert-Einstein-Institut, Max-Planck-Institut für Gravitationsphysik und Leibniz Universität Hannover*

Callinstraße 38
30167 Hannover, Germany

[3] *High Energy Physics Group, Physics Department, Imperial College London*

Blackett Laboratory, Prince Consort Road
London, SW7 2BW, UK

Corresponding author: Catia Grimani
catia.grimani@uniurb.it

[4]*DISPEA, Università di Urbino "Carlo Bo"*

Via S. Chiara, 27
61029 Urbino, Italy

[5]*INFN - Sezione di Firenze*

via G. Sansone 1
50019, Sesto Fiorentino, Firenze, Italy
[6]*APC, Univ Paris Diderot, CNRS/IN2P3, CEA/lrfu, Obs de Paris, Sorbonne Paris Cité, France*
[7]*Department of Industrial Engineering, University of Trento, via Sommarive 9, 38123 Trento, and Trento Institute for Fundamental Physics and Application / INFN*

[8]*Dipartimento di Fisica, Università di Trento and Trento Institute for Fundamental Physics and Application INFN*
38123 Povo, Trento, Italy
[9]*Istituto di Fotonica e Nanotecnologie, CNR-Fondazione Bruno Kessler, I-38123 Povo, Trento, Italy*

[10]*The School of Physics and Astronomy, University of Birmingham*
Birmingham, UK

[11]*Dipartimento di Fisica, Università di Trento and Trento Institute for Fundamental Physics and Application / INFN*
38123 Povo, Trento, Italy

[12]*Institut für Geophysik, ETH Zürich*

Sonneggstrasse 5
CH-8092, Zürich, Switzerland

[13]*Dipartimento di Scienze Fisiche e Chimiche, Università degli Studi dell'Aquila*

Via Vetoio, Coppito,
67100 L'Aquila, Italy

[14]*The UK Astronomy Technology Centre, Royal Observatory Edinburgh*

Blackford Hill, Edinburgh
EH9 3HJ, UK
[15]*Institut de Ciències de l'Espai (ICE, CSIC) Campus UAB, Carrer de Can Magrans s/n E-08193 Cerdanyola del Vallès Institut d'Estudis Espacial de Catalunya (IEEC) Edifici Nexus I, C/ Gran Capità 2-4, despatx 201 E-08034 Barcelona, Spain*

[16]*European Space Technology Centre, European Space Agency*

Keplerlaan 1
2200 AG Noordwijk, The Netherlands

[17]*European Space Operations Centre*

European Space Agency
64293 Darmstadt, Germany

[18]*Physik Institut, Universität Zürich*

Winterthurerstrasse 190
CH-8057 Zürich, Switzerland

[19]*SUPA, Institute for Gravitational Research*

School of Physics and Astronomy, University of Glasgow
Glasgow, G12 8QQ, UK
[20]*Nuclear Physics Institute of the CAS, Řež, Czech Republic*

[21]*Istituto di Astrofisica e Planetologia Spaziali*
INAF, Roma, Italy

[22] *Department d'Enginyeria Electrònica, Universitat Politècnica de Catalunya*
08034 Barcelona, Spain

[23] *Gravitational Astrophysics Lab, NASA Goddard Space Flight Center*

8800 Greenbelt Road
Greenbelt, MD 20771 USA

[24] *Osservatorio Astrofisico di Torino, INAF*
Pino Torinese, Italy

ABSTRACT

Non-recurrent short term variations of the galactic cosmic-ray (GCR) flux above 70 MeV n^{-1} were observed between 2016 February 18 and 2017 July 3 aboard the European Space Agency LISA Pathfinder (LPF) mission orbiting around the Lagrange point L1 at 1.5×10^6 km from Earth. The energy dependence of three Forbush decreases (FDs) is studied and reported here. A comparison of these observations with others carried out in space down to the energy of a few tens of MeV n^{-1} shows that the same GCR flux parameterization applies to events of different intensity during the main phase. FD observations in L1 with LPF and geomagnetic storm occurrence is also presented. Finally, the characteristics of GCR flux non-recurrent variations (peaks and depressions) of duration < 2 days and their association with interplanetary structures are investigated. It is found that, most likely, plasma compression regions between subsequent corotating high-speed streams cause peaks, while heliospheric current sheet crossing cause the majority of the depressions.

---

[*] Deceased 1 April 2017

[†] Deceased 20 January 2019

[‡] Deceased 30 September 2012

1. INTRODUCTION

Galactic cosmic rays (GCRs) show an almost isotropic spatial distribution in the inner heliosphere and consist of approximately 90% protons, 8% helium nuclei, 1% heavy nuclei and 1% electrons (percentages are in particle numbers to the total number). The overall GCR energy integral flux at 1 a.u. ranges approximately from 4000 particles $\mathrm{m^{-2}\ sr^{-1}\ s^{-1}}$ at solar minimum through 1000 particles $\mathrm{m^{-2}\ sr^{-1}\ s^{-1}}$ at solar maximum showing an eleven year quasi-periodicity (see for instance Papini, Grimani and Stephens 1996). During periods of negative solar polarity (when the global solar magnetic field lines enter the Sun North Pole) the flux of positively charged particles appears to be more modulated up to a maximum of 40% at 100 MeV $\mathrm{n^{-1}}$ at solar minimum, with respect to epochs of positive solar polarity (when the global solar magnetic field lines exit the Sun North Pole, Potgieter 2013). The GCR flux modulation during epochs of opposite solar polarities present a quasi-periodicity of twenty-two years (e. g. Laurenza et al. 2014, and references therein). In addition to these long-term GCR flux modulations, short-term variations ($\leq$ 1 month) associated with the passage of large-scale interplanetary structures are also observed (see for instance Richardson, Wibberenz and Cane 1996; Richardson 2004; Sabbah 2000, 2007; Sabbah and Kudela 2011; Armano et al. 2018a; Munini et al. 2018).

LISA Pathfinder (LPF) was the key technology demonstrator mission of the European Space Agency (ESA) Laser Interferometer Space Antenna (LISA), the first interferometer devoted to gravitational wave detection in space in the frequency interval 10^{-4} Hz - 10^{-1} Hz (Amaro-Seoane et al. 2017). The LPF spacecraft orbited around the Lagrange point L1 at 1.5 million km from Earth in the Earth-Sun direction. A high counting rate particle detector (PD; Cañizares et al. 2011), hosted aboard the LPF mission (Antonucci et al. 2011, 2012; Armano et al. 2016, 2018b) allowed for the measurement of the GCR integral proton and helium fluxes above 70 MeV $\mathrm{n^{-1}}$ from 2016 February 18 through 2017 July 3 during the descending phase of the present solar cycle N. 24 characterized by a positive polarity period of the Sun (Grimani et al. 2017; Armano et al. 2018a,c). The aim to place a PD aboard LPF was to measure the integral flux of particles of galactic and solar origin energetic enough to penetrate the spacecraft and charge the test masses that constitute the heart of the interferometer. Despite

the PD was not meant for scientific use, it was tested on beam experiment (Mateos et al. 2012) and the minimum energy of 70 MeV n^{-1} of ions crossing the detector was measured with high accuracy.

This manuscript focuses on the characteristics of three Forbush decreases (FDs) and of non-recurrent GCR flux short-term variations < 2 days observed during the LPF mission lifetime. FDs (Forbush 1937, 1954, 1958; Cane 2000) are sudden drops of the GCR flux intensity due the passage of interplanetary coronal mass ejections (ICMEs) and shocks. These GCR non-recurrent variations were primarily studied with the world wide neutron monitor (NM) network since the 1950s (see for instance Barouch & Burlaga 1975; Cane, Richardson and von Rosenvinge 1996), although only cosmic-ray flux measurements gathered in space (Lockwood et al. 1971) allow for the study of the energy-dependence of the depressed GCR flux down to a few tens of MeV without the use of models applied to Earth observations (Hofer and Flückiger 2000; Beer 2000; Usoskin, Bazilevskaya and Kovaltsov 2011; Usoskin et al. 2017). The LPF 2016 August 2 FD data (Armano et al. 2018a) are compared here to those of the satellite experiment PAMELA (Adriani et al. 2011; Usoskin et al. 2015; Munini et al. 2018). The ratio of the depressed to pre-decrease GCR fluxes during the main phase of the observed FDs is studied as a function of the energy.

FD, geomagnetic storm occurrence and the possibility of using FDs as precursor of geomagnetic activity was studied in the literature since early days (see for instance Lockwood et al. 1971; Badruddin and Kumar 2015; Chauhan, Manjula and Shrivastava 2011; Kane 2010). FD observations with LPF and contemporaneous geomagnetic activity are illustrated here.

The low statistical errors characterizing the data provided by the PD aboard LPF allowed also for the study of GCR flux non-recurrent variations (depressions and peaks) shorter than 2 days.

This manuscript is organized as follows: in Section 2 the characteristics of the PD hosted aboard LPF are described; in Section 3 the evolution of three FDs observed with LPF are compared to simultaneous measurements of solar wind parameters carried out in L1 and to NM observations placed at different geographic latitudes; in Section 4 parameterizations of proton and helium differential flux measurements gathered in space before and during the main phase of FDs are reported; in Section 5 a brief discussion on FDs and geomagnetic storm occurrence during LPF is presented and in Section

6 the association between interplanetary structures and <2 day GCR flux non-recurrent variations is illustrated.

2. THE PARTICLE DETECTOR ABOARD THE LPF SPACECRAFT

The LPF spacecraft was launched with a Vega rocket from the Kourou base in French Guiana on 2015 December 3. The satellite reached its final 6-month orbit around the first Lagrangian point L1 at the end of January 2016. The spacecraft elliptical orbit was inclined by about 45 degrees to the ecliptic. Minor and major axes of the orbit were approximately 0.5 million km and 0.8 million km, respectively.

Two nearly 2-kg cubic gold-platinum free-falling test masses played the role of mirrors of the interferometer aboard LPF. Cosmic-rays with energies larger than 100 MeV n^{-1} penetrated approximately 13 g cm^{-2} of spacecraft and instrument materials and charged the test masses. This process was expected to constitute one of the main sources of noise for LISA-like space interferometers in case of intense solar energetic particle events (Shaul et al. 2006; Armano et al. 2017a). A PD aboard LPF allowed for *in situ* monitoring of protons and helium nuclei of GCRs and solar particles. A shielding copper box of 6.4 mm thickness surrounded the silicon wafers in order to stop ions with energies smaller than 70 MeV n^{-1}. This conservative choice was made in order not to underestimate the overall incident particle flux charging the test-masses.

The LPF PD was mounted behind the spacecraft solar panels with its viewing axis along the Sun-Earth direction. It consisted of two ~ 300 μm thick silicon wafers of 1.40 x 1.05 cm^2 area, placed in a telescopic arrangement at a distance of 2 cm. This detector allowed for the counting of particles traversing each of the two silicon layers (single counts). Single counts were returned to the telemetry every 15 s. The energy deposits in the rear detector of particles traversing both silicon wafers in less than 525 ns (coincidence mode) were stored on the onboard computer in histograms of 1024 energy linear bins from 0 MeV to 5 MeV and returned to the telemetry every 600 seconds. The PD geometrical factor for particle energies > 100 MeV n^{-1} was of 9 cm^2 sr for single counts and about one tenth of this value for particles in coincidence mode. The maximum allowed detector counting rate was 6500 counts s^{-1} in the single count configuration. In coincidence mode 5000 energy deposits

per second was the saturation limit corresponding to an event proton fluence of 10^8 protons cm^{-2} at energies > 100 MeV.

The spurious test-mass acceleration noise due to the charging process was estimated before the mission launch with Monte Carlo simulations (Araújo et al. 2005; Grimani et al. 2005; Wass et al. 2005; Grimani et al. 2015) on the basis of GCR and solar energetic particle (SEP) flux predictions at the time the mission was supposed to be sent into orbit. The reliability of GCR flux predictions was positively tested with LPF data after mission end (Armano et al. 2018c) and with the Space Station AMS-02 magnetic spectrometer experiment (Aguilar et al. 2002) preliminary data above 400 MeV n^{-1} presented at COSPAR 2018 (2018 July 14-22, Pasadena, USA) and expected to be reported in a forthcoming publication of the AMS collaboration. No SEP events occurred during the LPF mission, nevertheless test-mass discharging was carried out periodically with ultraviolet light beams illuminating the capacitor system surrounding the test-masses (Armano et al. 2017a, 2018d) for acceleration noise control.

## 3. CHARACTERISTICS OF FORBUSH DECREASES OBSERVED WITH LISA PATHFINDER

The LPF 15-s proton and helium single counts gathered between 2016 February 18 and 2017 July 3 were hourly-averaged in order to set the statistical uncertainty of each data point to 1%. The percentage change (PC) of these measurements calculated with respect to their average value observed during each Bartels rotation (BR) was visually inspected over the LPF mission lifetime. This approach was adopted in order to limit the role of the solar modulation decrease during the years 2016-2017. It is recalled here that the BR number represents the number of 27-day periods of the Sun since 1832 February 8. The GCR flux variations were then compared to contemporaneous interplanetary magnetic field (IMF) and solar wind plasma parameters gathered by the ACE experiment (Stone et al. 1998) orbiting around the Lagrange point L1 (https://cdaweb.sci.gsfc.nasa.gov/index.html).

The passage of near-Earth ICMEs (reported in http://www.srl.calctech.edu/ACE/ASC/DATA/level3/icmetable2.htm) was associated with three FD observations carried out with the LPF PD on 2016 July 20, 2016 August 2 (for this event see also Armano et al. 2018a) and 2017 May 27 as it is shown in the left Figures 1-3. In these figures the GCR flux variations are compared to the

solar wind speed (V), to the IMF sunward x component in the GSE coordinate system with opposite sign ($-B_x$) observed to match the sector polarity and to the IMF intensity (B). The ICME passage is marked by dashed lines. The FD dated 2016 July 20 is associated with both solar wind speed and IMF increases due to the ICME propagating into a previous corotating high-speed solar wind stream (CHSS, V$>>$ 400 km s^{-1}). On 2016 August 2 and 2017 May 27 the GCR flux modulations appear correlated with the IMF intensity increase only. In all three cases the IMF intensity presented maximum values of about 25 nT.

In order to study the energy dependence of the three FDs observed with LPF, the PC of the integral proton and helium fluxes measured with the PD above 70 MeV n^{-1} were compared to contemporaneous hourly-averaged PC of observations gathered with NMs located at different geographic latitudes in the right Figures 1-3 (www.nmdb.eu, a similar attempt for NMs only was carried out in Badruddin and Kumar (2015)). The GCR flux PC observed aboard LPF or with NMs was calculated by using as baseline (PC=0%) the average values of counts measured by PD or NMs during the BR to which the studied period of time belongs. The Terre Adelie, Oulu, Rome and Mexico NM stations are characterized by geomagnetic cut-off rigidities of 0 GV, 0.8 GV, 6.3 GV and 8.2 GV, respectively. The shielding effect of the atmosphere and the geomagnetic cut-off do not allow NMs of providing direct measurements of GCR energy spectra at low energies. Conversely, the PC of NM counting rate measured on Earth is approximately the same of the GCR integral flux incident at the top of the atmosphere above *effective energies*. Effective energies range from 11-12 GeV for polar stations through 20 GeV for equatorial stations (see for details Gil et al. 2017, and references therein). In Table 1 are reported the PC of the GCR integral flux observed with LPF and with the NMs listed above, at the maximum of each FD. Time of the onset and of the maximum of each FD aboard LPF are also indicated. The onset was set as the first time bin after which the GCR flux presented a continuous decrease trend, within statistical uncertainty, for at least six hours. The time when the GCR integral flux reached its minimum value during each FD was estimated with a best line fit through the data points. The LPF proton-dominated (resulting from proton and helium measurements) integral flux maximum decreases above 70 MeV were observed to vary from about
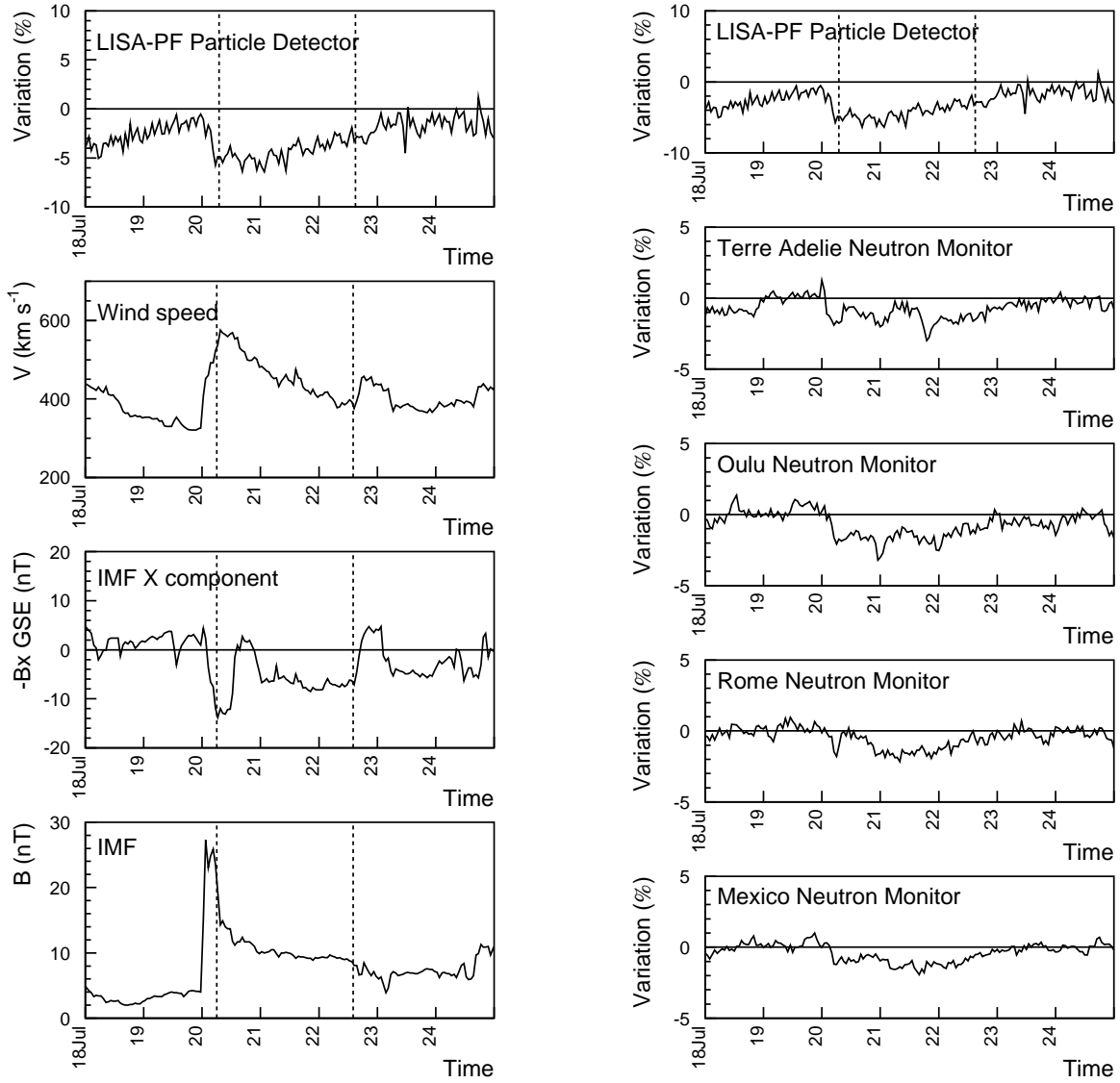
Figure 1. Left: The LPF PD GCR hourly averaged counting rate PC between 2016 July 18 and 2016 July 24 are reported in the top panel. The solar wind speed (V) is shown in the second panel. The Geocentric Solar Ecliptic (GSE) coordinate system sunward IMF x-component with opposite sign (-B_x) and IMF intensity (B) appear in the third and fourth panel, respectively. The IMF and solar wind parameter data were gathered from the ACE experiment (https://cdaweb.sci.gsfc.nasa.gov/index.html) in the Lagrange point L1. The passage of a near-Earth ICME is indicated by vertical dashed lines (http://www.srl.caltech.edu/ACE/ASC/DATA/level3/icmetable2.htm). A FD is observed to begin on July 20. Right: Comparison of LPF hourly-averaged GCR counting rate PC with contemporaneous, analogous measurements of NMs placed at various geographic latitudes (www.nmdb.eu). Dashed lines in the top panel have the same meaning as those in the left figures.
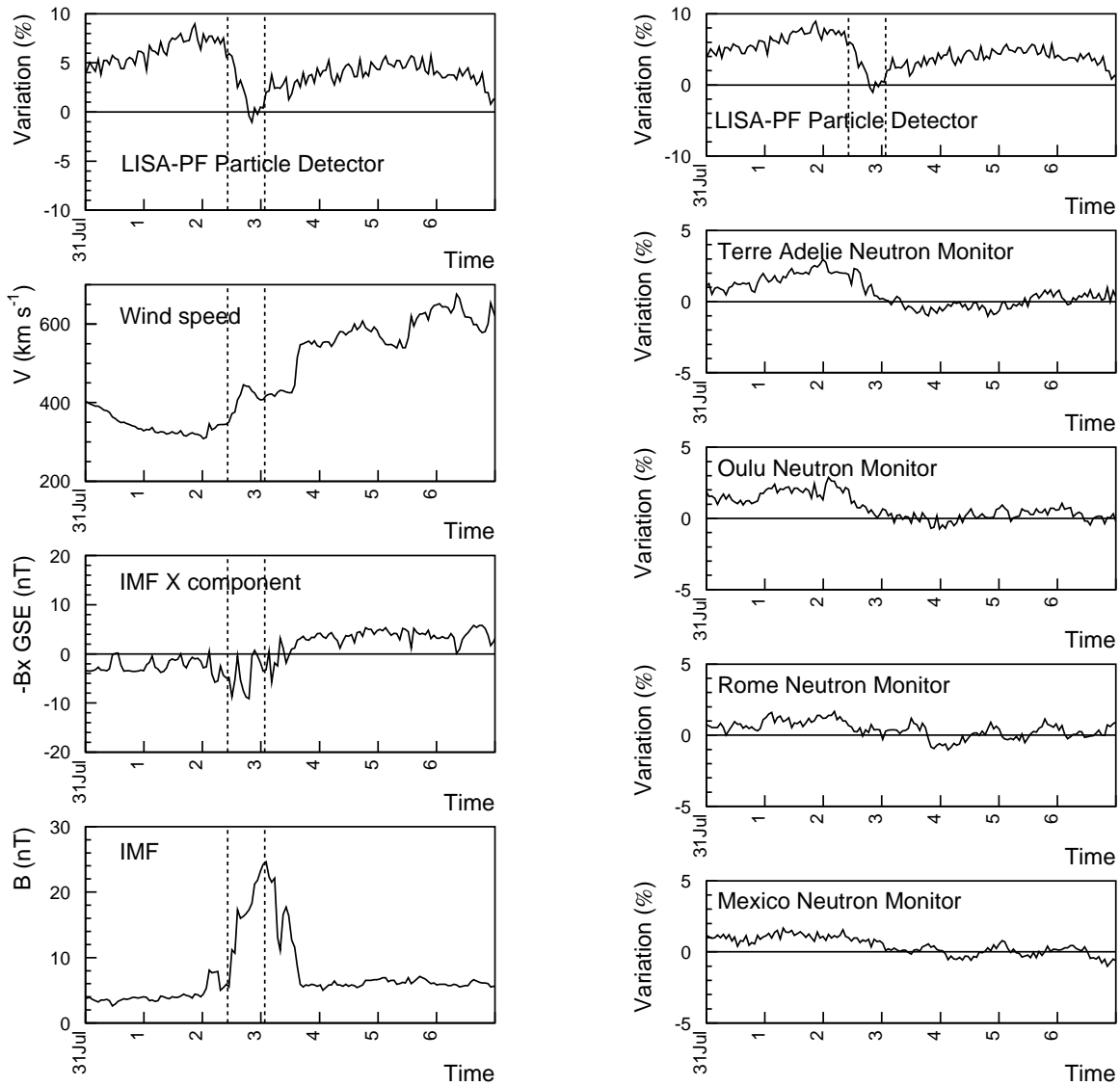
Figure 2. Same as Figure 1 for the period 2016 July 31 - 2016 August 6.

5% to 9% during the three events. The different GCR flux decrease observed with LPF in response to similar IMF intensity increases is most likely due to the passages of interplanetary structures that depressed the GCR flux before the transit of the ICMEs. During the 2016 August 2 event only, the pre-decrease GCR flux appeared at its maximum value during the BR 2496 before the passage of the ICME that generated the FD (see Figure 7 in Armano et al. (2018a)). NM data show PCs above effective energies ranging between 1% and 3%. Both GCR flux main and recovery phases
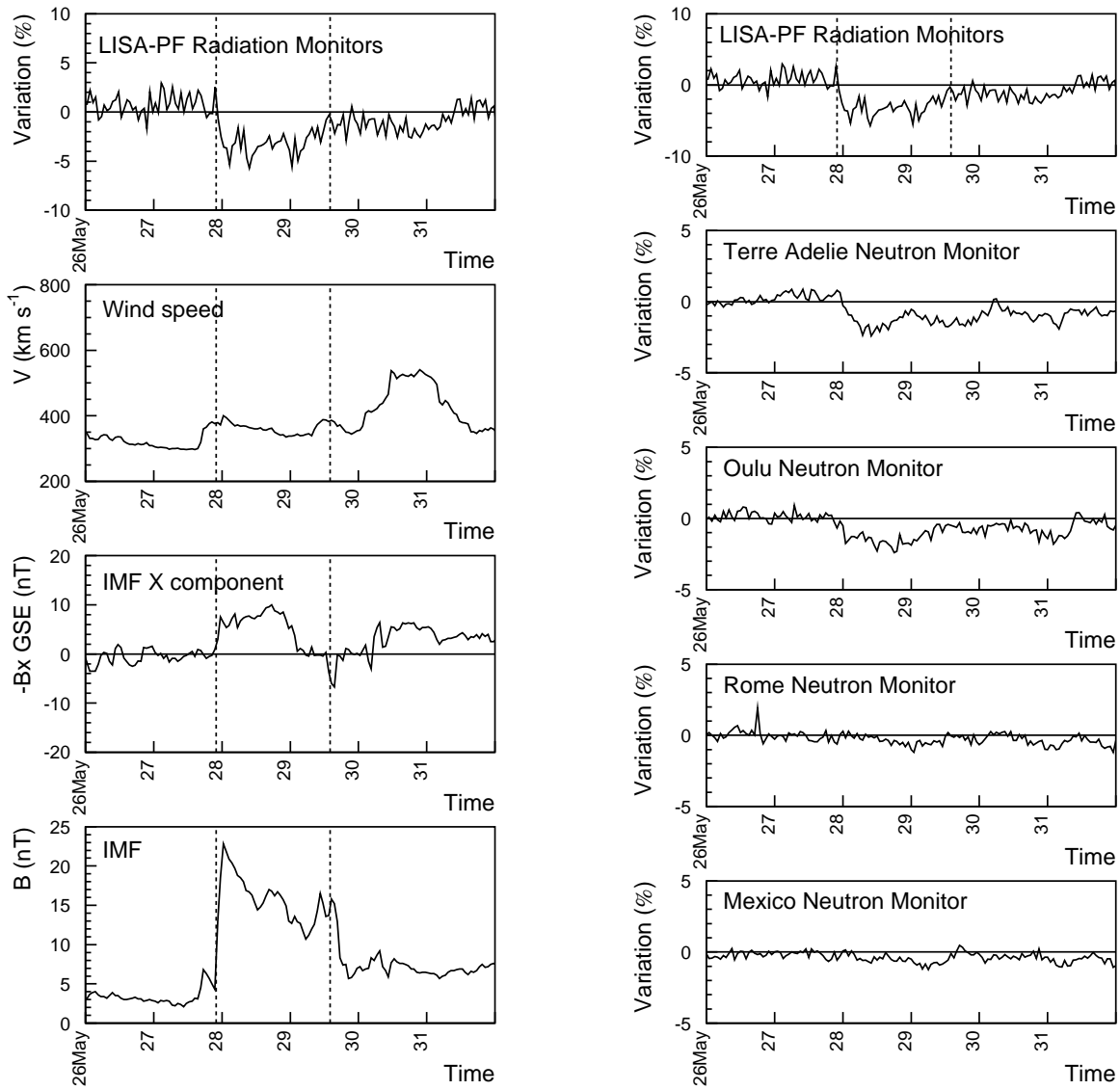
Figure 3. Same as Figure 1 for the period 2017 May 26 - 2017 May 31.

are observed in all considered NM measurements during the 2016 July 20 FD. This is not the case for the other two events that can be clearly detected in polar NM measurements only. The energy dependence of GCR flux depressions during FDs was also discussed, for instance, in Usoskin et al. (2008); Grimani et al. (2011); Badruddin and Kumar (2015).

Table 1. Energy dependence of the GCR integral flux PC at the maximum of the three FDs observed aboard LPF above 70 MeV n^{-1} and with NMs above effective energies: 11 GeV for polar stations; 12 GeV for Oulu NM; 17 GeV for Rome NM and 20 GeV for Mexico NM

LPF FD onset Time	LPF FD maximum Time	PC > 70 MeV	PC > 11 GeV	PC > 12 GeV	PC > 17 GeV	PC > 20 GeV
2016 July 20 07.00 UT	July 21 01.00 UT	5.5%	2%	2%	2%	1%
2016 August 2 12.00 UT	August 2 22.40 UT	9%	3%	2%	2%	1%
2017 May 27 18.00 UT	May 28 10.45 UT	7%	3.5%	2.5%	1%	1%

The transit of other three near-Earth ICMEs on 2016 March 5, 2016 April 14 and 2016 October 13 resulted in GCR flux decreases at the limit of the statistical significance (1-2%) on LPF, the GCR flux being already reduced by the transit of previous interplanetary structures and heliospheric current sheet crossing (HCSC; see Figure 6 in Armano et al. (2018a) and Figure 4).

4. PARAMETERIZATION OF GCR ENERGY SPECTRA DURING FDS

GCR flux measurements gathered in space are considered in this Section to investigate if the same parameterization could be used to replicate the trend of the GCR flux PC during the main phase of FDs of different intensity. The LPF GCR observations gathered before and at the maximum (22.40 UT) of the 2016 August 2 FD are compared to those of the satellite PAMELA experiment, which measured both proton and helium differential fluxes before and during the main phase of the FD dated 2006 December 14 between 16.50 UT and 22.35 UT (see for details Adriani et al. 2011; Usoskin et al. 2015; Munini et al. 2018). The PAMELA data can be found in https://tools.ssdc.asi.it/CosmicRays/. In Figure 5 vertical solid lines delimit the interval of time during which PAMELA observed the FD. The pre-decrease and depressed proton energy spectra observed by PAMELA in November 2006 and on 2006 December 14, respectively, are shown in Figure 6. The PAMELA data are reported in https://tools.ssdc.asi.it/CosmicRays/. In the same figure, pre-decrease and depressed proton
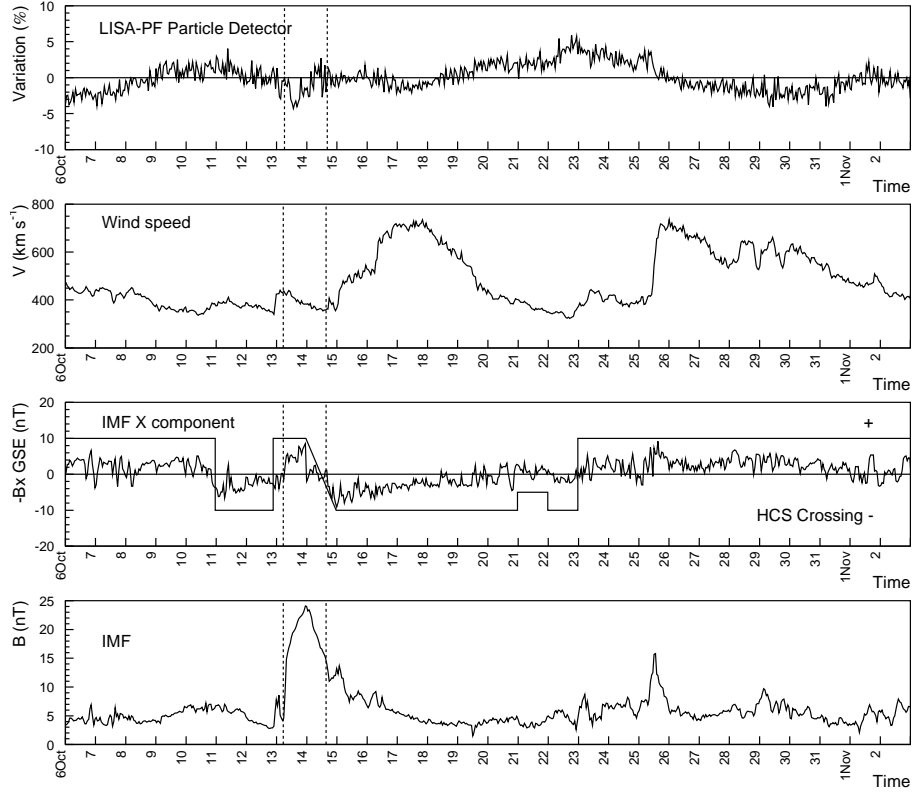
Figure 4. From top to bottom panels: GCR flux variations aboard LPF; solar wind speed (V), IMF negative component (-B$_x$) in GSE coordinate system and IMF intensity (B) during the BR 2499 (2016 October 6 - 2016 November 1). In panel 3 the continuous line indicates HCSC and sector daily polarity (positive and negative polarities were set to +10 and -10 arbitrarily in the plot). Undefined polarities were equally arbitrarily set to +5 and -5 (sector polarities are reported in http://omniweb.sci.gsfc.nasa.gov./html/polarity/polarity_tab.html). The passage of a near-Earth ICME is indicated by vertical dashed lines (http://www.srl.caltech.edu/ACE/ASC/DATA/level3/icmetable2.htm).

dominated energy differential fluxes for the FD dated 2016 August 2 are also reported. The PAMELA data gathered during the main phase of the FD are not shown below 500 MeV since the proton flux included particles of both galactic and solar origin. It is pointed out that the PAMELA pre-decrease flux measurements were considered those gathered in 2006 November since the solar modulation during the months of 2006 November and 2006 December was very similar
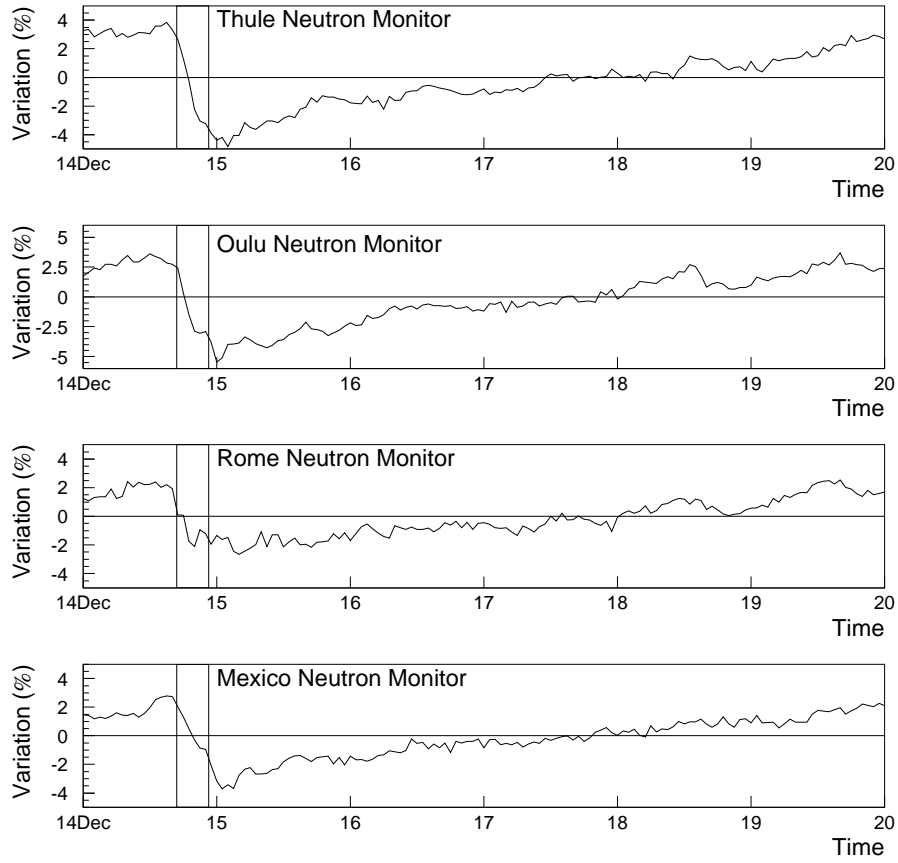
Figure 5. NM measurements at various geographic latitudes between 2006 December 14 and 2006 December 19. A FD on December 14 was also observed in space by the satellite experiment PAMELA above 70 MeV n^{-1} from 16.50 UT through 22.35 UT on 2006 December 14 (vertical continuous lines).

(http://cosmicrays.oulu.fi/phi/Phi_mon.txt). PAMELA helium data for the same FD appear in Fig. 7.

The energy spectra of cosmic rays observed during the main phase of the FDs ($F_{FD}(E)$) considered in this Section and corresponding pre-decrease energy spectra (F(E)) are parameterized as indicated in eqs. 1 and 2 (Papini, Grimani and Stephens 1996), respectively:

$$F_{FD}(E) = A \ (E + b')^{-\alpha} \ E^{\beta} \quad \text{particles (m}^2 \text{ sr s GeVn}^{-1})^{-1}, \tag{1}$$
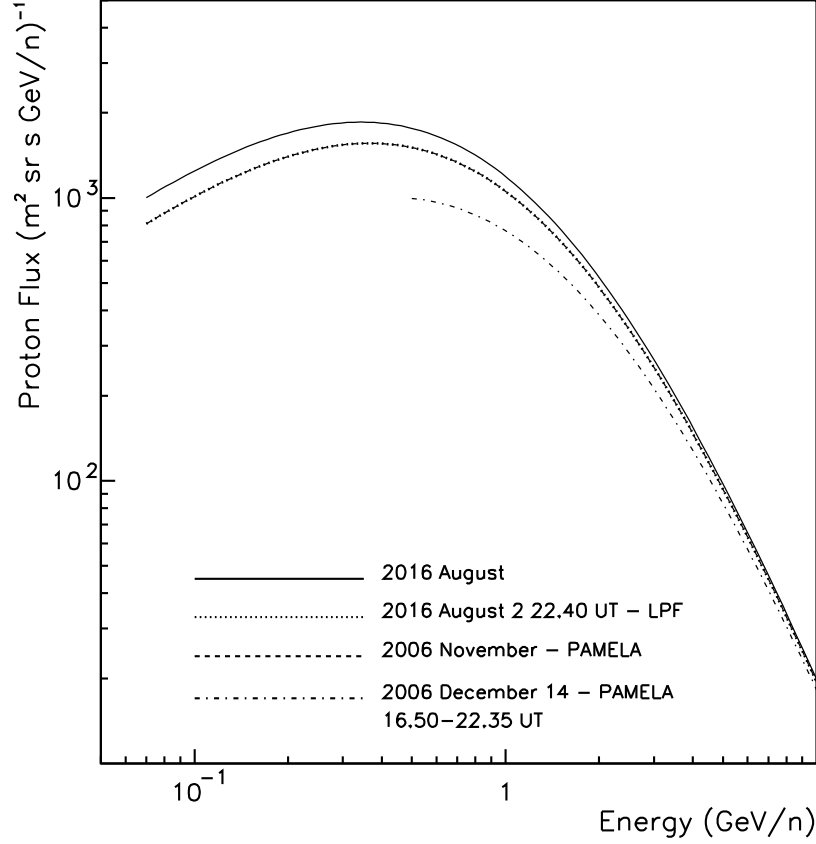
Figure 6. Proton energy spectra measured by the PAMELA experiment before (dashed line) and during the FD dated 2006 December 14 (dot-dashed line). The proton-dominated observations carried out with LPF and NMs on 2016 August 2 at the maximum of the FD (22.40 UT) are also shown (dotted line). The 2016 August pre-decrease proton flux is represented by a continuous line. The depressed proton spectrum observed during the August 2 FD with LPF superpose to the pre-decrease proton flux measured by PAMELA in November 2006.

$$F(E) = A \ (E + b)^{-\alpha} \ E^{\beta} \quad \text{particles } (\text{m}^2 \text{ sr s GeV n}^{-1})^{-1} \tag{2}$$

with $b' > b$. The parameters α and β remain unchanged since these parameters modulate the GCR flux above 10 GeV where pre-decrease and depressed fluxes present approximately the same slope as it can be observed in Figures 6 and 7. The parameterizations reported in eqs. 1 and 2 are found to reproduce the GCR energy spectra trend in the inner heliosphere in the energy range of observations
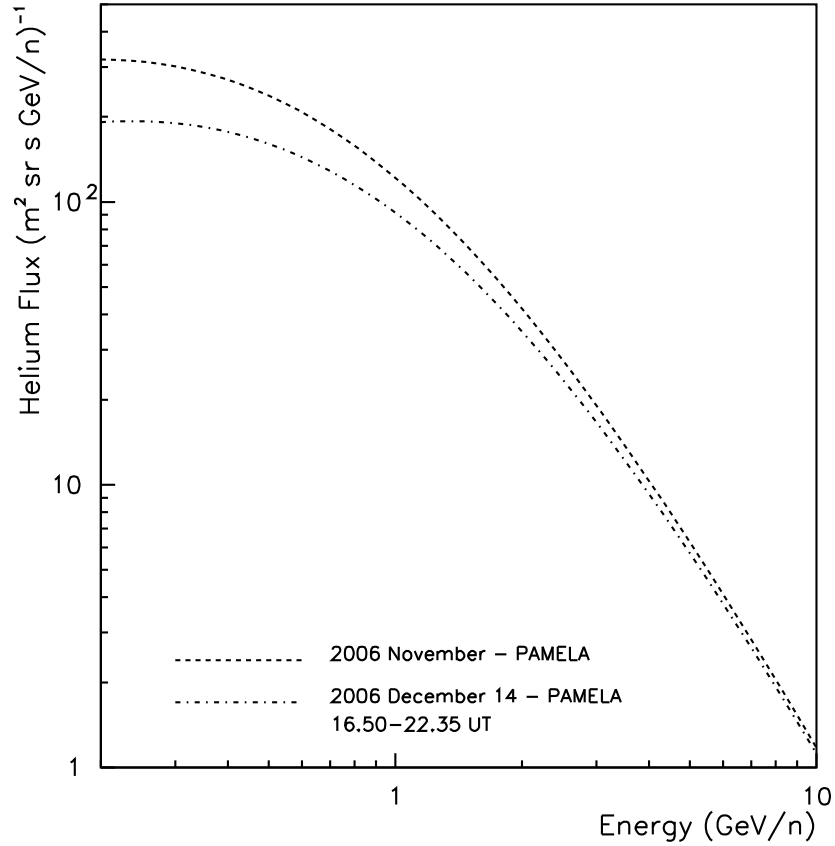
Figure 7. Helium energy spectra measured by the PAMELA experiment before and during the FD dated 2006 December 14.

between a few tens of MeV n^{-1} up to hundreds of GeV n^{-1} in agreement with the Gleeson and Axford model (Gleeson and Axford 1968) within experimental errors of data. These parameterizations are adopted in this work instead of using the model by Gleeson and Axford during FDs (see for instance Usoskin et al. 2015), since in this last model the modulation of GCR energy spectra is correlated with the solar modulation parameter that follows the long-term quasi-periodicity of the solar activity. The solar modulation parameter is kept here constant during each BR and it is preferred to increase the parameter b (in eq. 2) to b' (in eq. 1) to reproduce the observed GCR flux trend during a FD to decouple the effects of long and short-term GCR flux variations.

The parameters A, b, b', α, β estimated for each data set are indicated in Table 2. The χ^2 and number of degrees of freedom for each parameterization of the PAMELA data (available in https://tools.ssdc.asi.it/CosmicRays) are also reported in Table 2. For the 2016 August 2 LPF FD the pre-decrease proton differential flux above 70 MeV was estimated on the basis of the Gleeson and Axford model by assuming a solar modulation parameter of 438 MV (http://cosmicrays.oulu.fi/phi/Phi_mon.txt) for the 2016 August month and the interstellar proton spectrum by Burger, Potgieter and Heber (2000). The differential flux thus obtained was then parameterized as indicated in eq. 2 and integrated above 70 MeV and above the effective energies of polar, Oulu, Rome and Mexico NM stations. The integral flux values were then reduced at 70 MeV and at effective energies as observed by LPF at 22.40 UT of 2016 August 2 and by NMs between 22.00 and 23.00 UT of the same day. Finally, the differential flux at the maximum of the FD was estimated by increasing the parameter b of the pre-decrease differential flux (third raw in Table 2 and eq. 2) to b' (fourth raw in Table 2 and eq. 1) until obtaining an agreement to better than 1% between the modulated integral flux and integral flux measurements carried out with LPF and NMs. No χ^2 was calculated for LPF since no differential flux measurements are available for our experiment. In Armano et al. (2018a) the same approach presented here was adopted by using, however, the Shikaze et al. (2007) interstellar proton spectrum inferred from the BESS experiment data gathered during both positive and negative polarity periods of the Sun. The solar modulation parameter values obtained with the BESS data differ from those reported in http://cosmicrays.oulu.fi/phi/Phi_mon.txt obtained with the Burger, Potgieter and Heber (2000) interstellar spectra only by a few tens of MV, considered to lie within the uncertainty of the method. After the publication of the AMS experiment data gathered during the month of August 2016, it will be possible to set the uncertainties on the outcomes of the present work.

By defining R(E) the ratio of the GCR flux interpolations that appear in eqs. 1 and 2, respectively:

$$R(E) = \frac{F_{FD}(E)}{F(E)}, \tag{3}$$

it is found:

Table 2. Parameterizations of proton (p) and helium (He) energy spectra measured by the indicated experiments before and during Forbush decreases (see eqs. 1 and 2). The χ^2 and number of degrees of freedom ($ndof$) estimated for each set of experimental data are indicated.

	A	b	b'	α	β	χ^2	$ndof$
p (PAMELA experiment - 2006 November)	18000	1.17		3.66	0.87	2279.1	71
p (FD - 2006 December 14 16.50 UT - 22.35 UT)	18000		1.37	3.66	0.87	4948.7	71
p (LPF - 2016 August)	18000	1.10		3.66	0.87	-	-
p (2006 August 2 22.40 UT)	18000		1.17	3.66	0.87	-	-
He (PAMELA experiment - 2006 November)	850	0.75		3.47	0.72	16.38	18
He (FD - 2006 December 14 16.50 UT - 22.35 UT)	850		0.90	3.47	0.72	10.98	18

$$R(E) = \left(\frac{E + b'}{E + b} \right)^{-\alpha}. \tag{4}$$

R(E) estimated for LPF and PAMELA proton measurement interpolations are shown in Figure 8 while in Figure 9, R(E) was calculated for the PAMELA helium observation interpolations. The simple relationship in eq. 3 allows for a quick, even though approximate, estimate of the GCR energy differential flux during the main phase of a FD when integral flux measurements during the event evolution and the differential flux before the occurrence of the same are known.

The b/b' ratios of the parameters estimated with the GCR flux parameterizations before and during the main phase of each FD studied in this Section (two data points were considered for the FD dated 2006 December 14 since PAMELA measured both proton and helium fluxes) appear correlated with the GCR flux percentage attenuation (PA) as it is shown in Figure 10 (solid dots). PA is defined as follows:

$$PA = \frac{\int F_{FD}(E)dE}{\int F(E)dE}, \tag{5}$$
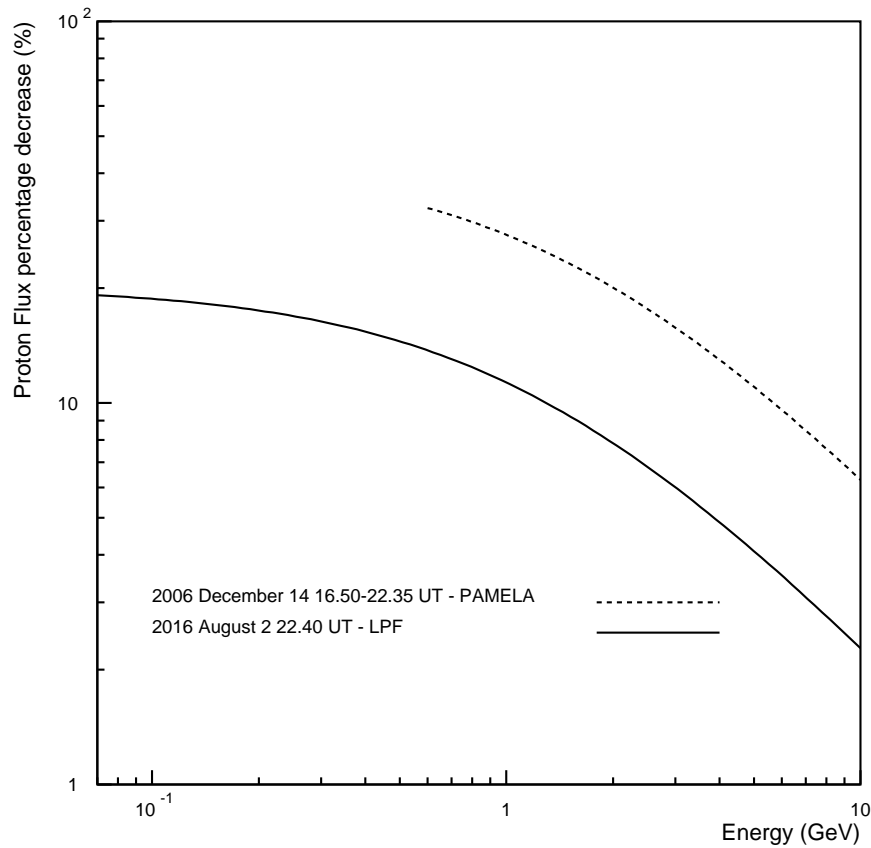
Figure 8. Parameterization of the proton flux percentage decrease observed by PAMELA and LPF during the main phase of the FDs dated on 2006 December 14 and 2016 August 2, respectively.

where integrals are calculated in the energy range of data availability during each event.

In Figure 11 the continuous line indicates the best fit through the data points. If additional observations gathered in space will confirm the reliability of this simple empirical relationship, it will be possible to set a statistical significance for the same.

5. FD OBSERVATIONS IN THE LAGRANGE POINT L1 AND GEOMAGNETIC STORM OCCURRENCE

Fifteen near-Earth ICMEs were observed (http://www.srl.caltech.edu/ACE/ASC/DATA/level3 /icmetable2.htm) during the time the LPF spacecraft was orbiting around the Lagrange point L1. Eight of these ICMEs presented magnetic clouds. As it was anticipated in Section 3, the GCR integral
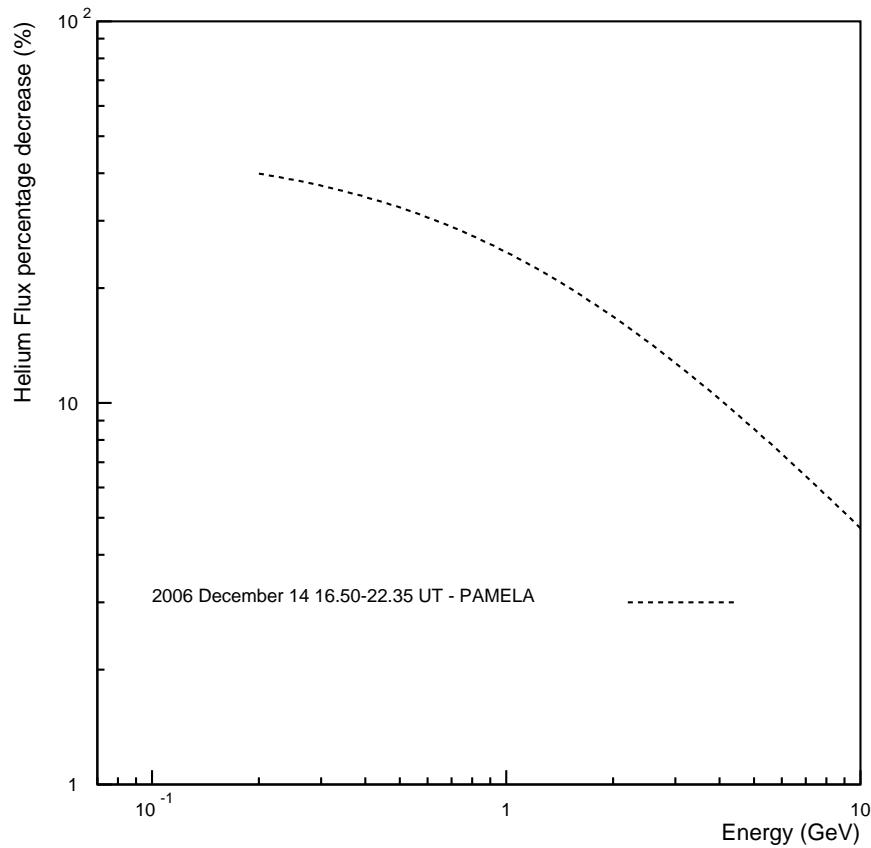
Figure 9. Parameterization of the percentage decrease of the helium flux observed by the PAMELA experiment during the FD dated on 2006 December 14.

flux measurements aboard LPF presented depressions at the time of the passage of six of these ICMEs (2016 March 5; 2016 April 14; 2016 July 20; 2016 August 2, 2016 October 13 and 2017 May 27) but in three cases only (on 2016 July 20, 2016 August 2 and 2017 May 27) FDs were observed. During the main phases of these three FDs the GCR flux decreases appeared correlated with the increase of the IMF intensity up to about 25 nT associated with the contemporaneous transit of ICMEs (see also Benella et al. 2019) while the solar wind speed remained below 400 km s^{-1} except at the onset of the 2016 July 20 event. Conversely, during the GCR flux depressions observed on 2016 March 5 (Figure 6 in Armano et al.; 2018a) and 2016 April 14 (Figure 11) the effects of ICME passages (from 19.00 UT on March 5 through 15.00 UT on March 6 and 09.00 UT on April 14 through 04.00 UT on April
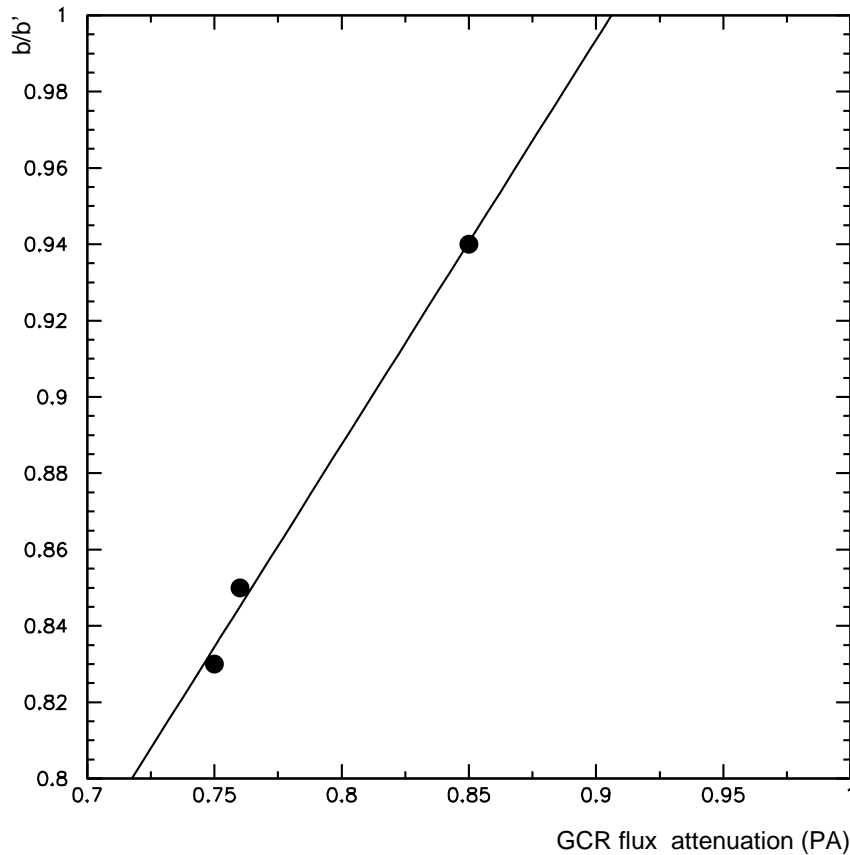
Figure 10. Parameterization of the b/b' ratio inferred from eqs. 1 and 2 for the FDs studied in this Section versus the GCR flux percentage attenuation (PA). The continuous line indicates the best-fit of the data points: b/b'=1.061 PA+0.0387.

15, respectively) were mainly concealed by the action of concomitant transits of several CHSS. On 2016 October 13 the role of a near-Earth ICME passage (from 2016 October 13 at 6.00 UT through 2016 October 14 at 16.00 UT; dashed lines in Figure 4) and increase of the IMF intensity > 20 nT in modulating the GCR flux could not be established since the GCR flux presented a continuous decreasing trend well before the passage of the ICME due to a previous transit of high-speed solar wind streams and HCSC on October 11, October 13 and October 14.

Geomagnetic storms are disturbances of the Earth's magnetosphere classified on the basis of their intensity by changes in the Dst (disturbance storm time) geomagnetic index representing the av-

erage change of the horizontal component of the Earth's magnetic field at the magnetic equator
(Gonzales et al. 2014). Geomagnetic storms are defined weak when the Dst ranges between -30 nT
and -50 nT; moderate when the Dst varies between -50 nT and -100 nT and strong when the Dst
is smaller than -100 nT. Moderate geomagnetic storms, more frequent than strong ones, affect com-
munications while the most intense ones may induce severe damages in critical infrastructures on
Earth. Near-Sun coronal mass ejection and near-Earth solar wind parameters are used to forecast
geomagnetic storms (Kim et al. 2014). The geomagnetic index Dst reached a value smaller than -100
nT twice during the period LPF collected data (2016 February 18 - 2017 July 3): on 2016 October
13 at 17.30 UT (-104 nT) and on 2017 May 28 at 07.30 UT (-122 nT). In Figure 12 it is shown that
no FD can be observed beyond statistical fluctuations with LPF and NMs. Conversely, the passage
of a near-Earth ICME was at the origin of both the FD observed on LPF and NMs on 2017 May
27-28 (Figure 3) and the geomagnetic storm occurred on 2017 May 28. The 2016 August 2 FD onset
occurred at 12.00 UT aboard LPF, about ten hours before a weak geomagnetic storm (Dst $\simeq$ -50 nT)
that started at 22.00 UT when the FD reached its maximum in the Lagrange point L1 (see Figure 7
in Armano et al. 2018a). For this event the geomagnetic storm and the maximum of the FD occurred
at the same time even though this is not a general result (see Kane 2010, for instance). Geomagnetic
storms are caused by fast solar wind streams and large negative values of the B_z component of the
IMF reconnecting with the Earth magnetic field while FDs are caused by large increases of the IMF
intensities. FD observations with LPF in the Lagrange point L1 and geomagnetic storm occurrence
are summarized in Table 3 along with maximum values of the observed IMF intensity and minimum
values of the B_z component during each FD. It can be concluded that FDs, when observed, can be
used to forecast geomagnetic storms only when the z-component of the IMF presents values < -20
nT (see also Dremukhina et al. 2011).

6. GCR FLUX NON-RECURRENT VARIATIONS < 2 DAYS DURING LPF

Data visual inspection of the whole LPF data set revealed the presence of several non-recurrent
substructures in the GCR flux of duration shorter than two days. A dedicated analysis was carried
out to investigate the characteristics and the origin of these variations. GCR flux depressions and

Table 3. FD observations and geomagnetic storm occurrence during the LPF mission.

Date	FD	Geomagnetic storm	Maximum B	Minimum Bz	Dst
	Yes/No	Yes/No	nT	nT	nT
2016 July 20	Yes	No	25	-8.9	> -50
2016 August 2	Yes	No	24	-9.5	$\simeq$ -50
2016 October 13	No	Yes	24	-19	-102
2017 May 27	Yes	Yes	23	-21	-122
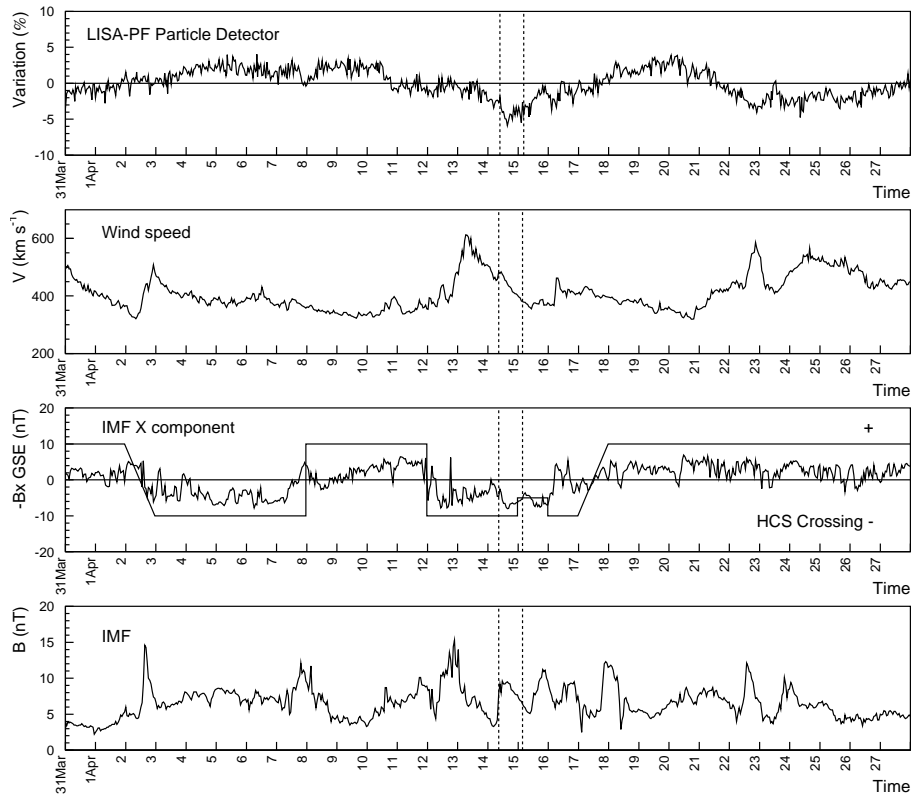
Figure 11. Same as Figure 4 for the BR 2492 (2016 March 31 - 2016 April 26).

peaks of duration longer than 0.75 days (18 hours) with intensities $> 2\%$ were studied. GCR flux variations larger than 2% in intensity were considered in order to set the statistical significance of the selection criterion to 2-σ, being of 1% the statistical uncertainty on PD hourly averaged single count data. The LPF PD observations during each BR were compared to the IMF intensity, solar wind plasma parameters and NM measurements. Twenty-three, non-recurrent < 2-day duration GCR flux variations were observed between 2016 February 18 and 2017 July 3. These twenty-three variations consisted of six enhancements and seventeen depressions. As an example, in Figure 11 data gathered during the BR 2492 present a small depression on 2016 April 7-8 and two small peaks on 2016 April 15 and April 23. A comparison of the LPF data with those gathered with polar NMs during the same BR 2492 in Figure 13 shows that the small GCR flux enhancement dated April 15 was observed in the most of the polar NM measurements, similarly the depression dated 7-8 April is observed by the Thule and McMurdo NMs. Conversely the April 23 enhancement is not observed in polar NMs. Interplanetary plasma (solar wind bulk speed, temperature and proton density) and magnetic field parameters are studied to identify interplanetary structures associated with individual <2-day GCR flux variations. In Table 4 CHSS, observed during subsequent Bartels rotations and originating from coronal holes, are characterized by a solar wind speed > 400 km s^{-1}, low magnetic field and plasma densities. Corotating interaction regions (CIR) are identified as regions of compressed plasma formed between the leading edges of CHSS at the interface that separates slow and fast stream plasma. Magnetic barriers (MBs) indicate those regions of high plasma magnetic field intensity observed between closely spaced CHSS. MFE stays for magnetic field enhancements in the slow solar wind. The majority of small depressions in the GCR flux are caused by HCSC; only seldom their evolution was modulated by CHSS and CIR. These findings resulted to be different from those obtained with an analogous study carried out in Armano et al. (2018a) for GCR flux recurrent depressions > 2 days indicating that, in general, these depressions are associated with CIR and with the passage of CHSS. Peaks with duration < 2 days appear associated with regions of compressed plasma between two CHSS (see for instance 2016 April 23-24 in Figure 12). Several processes may generate these small peaks in the GCR flux. The most plausible is that the lowest energy GCRs ($\simeq$

70 MeV) are excluded from regions of enhanced IMF intensity between subsequent CHSS. However, a change of the low-energy GCR spectrum slope between flux recovery phase after a CHSS passage and a new GCR flux decrease due to the passage of a subsequent CHSS may also generate a peak feature in the integral flux. An increase of the GCR flux due to the acceleration at the shock of incoming CHSS does not appear plausible on the basis of the absence of small peak structures at the passage of isolated CHSS (see Figure 6 in Armano et al. (2018a)). As a matter of fact, both models and observations indicate that the maximum energy of particles accelerated at CIR regions is about 20 MeV (Mc Donald et al. 1975; Bones and Simpson 1976; Tsurutani et al. 1985; Desai et al. 1998; Giacalone, Jokipii and Kóta 2000; Richardson 2004; Laurenza et al. 2015).

Table 4. Occurrence and characteristics of the GCR flux variations < 2 days observed with LPF . Interplanetary structures associated with each GCR flux < 2-day variation are indicated (CIR: corotating interaction region; CHSS: corotating high-speed solar wind streams; HCSC: heliospheric current sheet crossing; MFE: magnetic field enhancement in the slow solar wind; MB: low-energy cosmic rays confined in regions of high magnetic field between two subsequent CHSS). IMF, solar wind plasma data and near-earth ICME passages were gathered from the websites `https://cdaweb.sci.gsfc.nasa.gov/index.html` and `http://www.srl.caltech.edu/ACE/ASC/DATA/level3/icmetable2.htm`. HCSC are reported in `http://omniweb.sci.gsfc.nasa.gov./html/polarity/polarity_tab.html`.

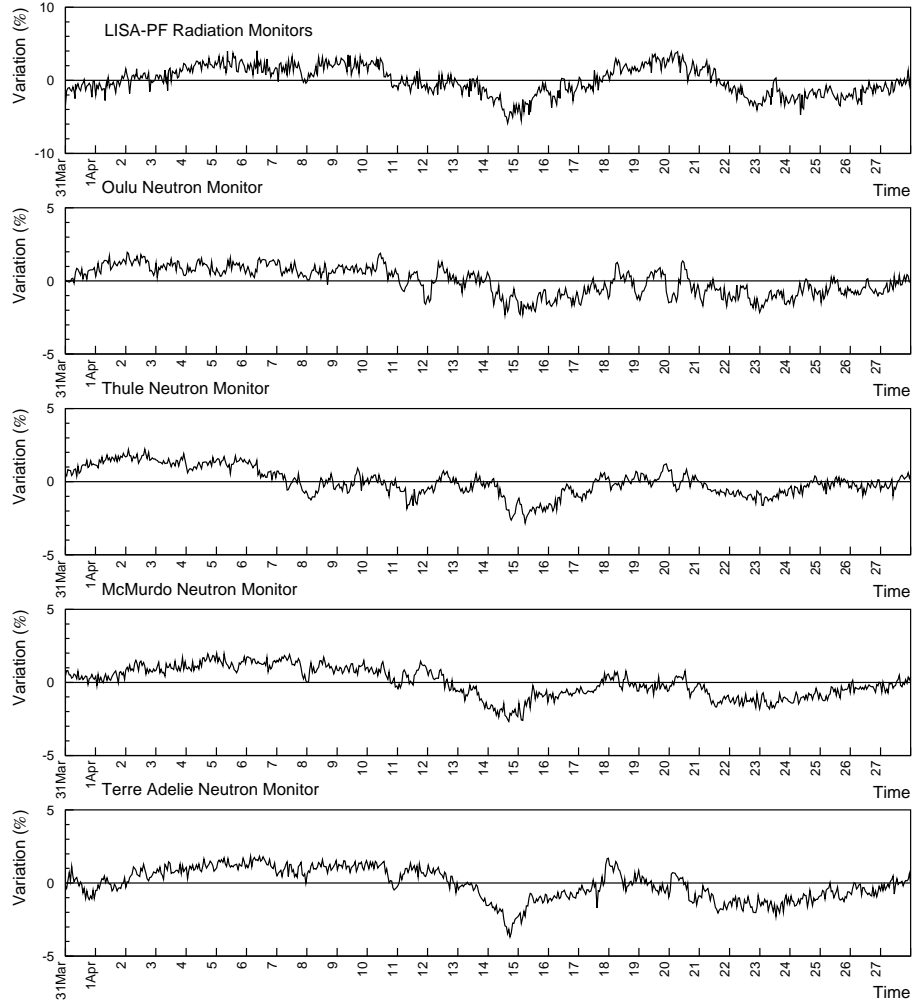| Date	Onset	Duration	Dip/Peak	Amplitude	Interplanetary structure
	Time	Days		%	
2016 March 11	7.44 UT	0.97	DIP	3.1	CIR+HCSC
2016 March 16	1.38 UT	0.84	PEAK	3.0	MB
2016 March 19	9.21 UT	1.16	DIP	2.5	CHSS
2016 April 7	16.31 UT	0.89	DIP	3.4	HCSC
2016 April 15	7.44 UT	0.75	PEAK	4.4	MB

Table 4 continued on next page
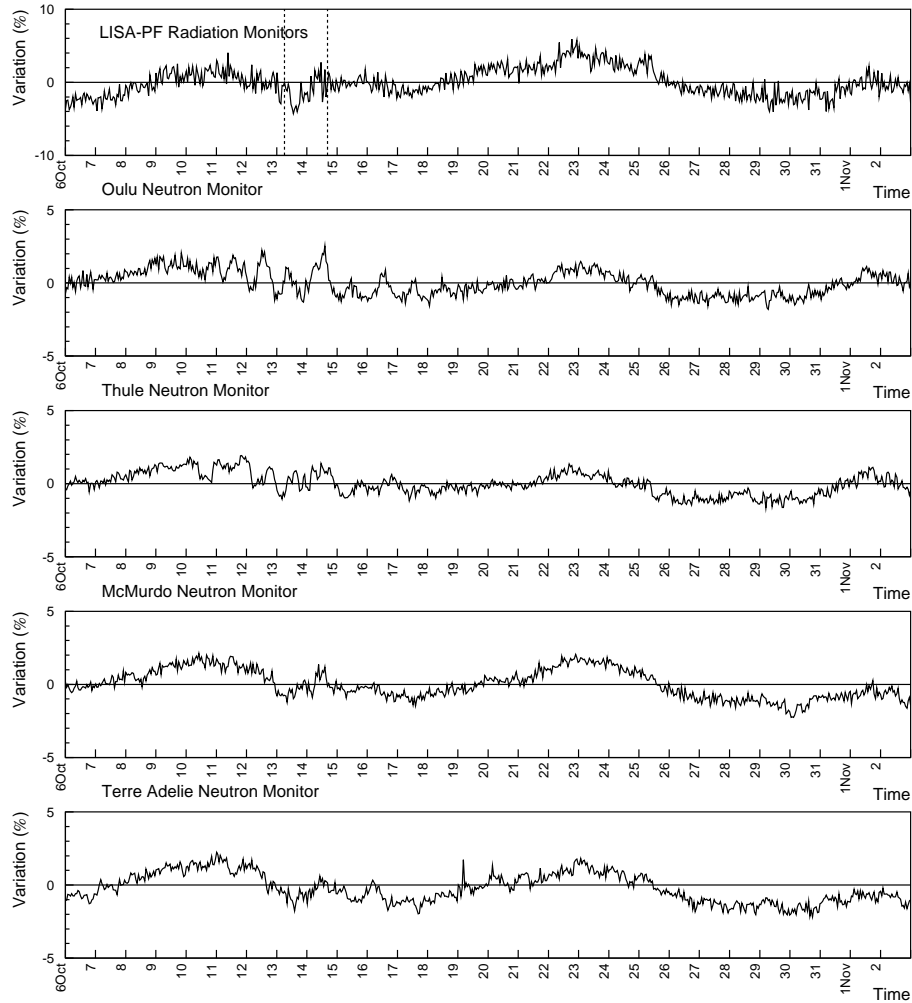
Figure 12. Comparison of LPF hourly-averaged GCR counting rate PC (top panel) with contemporaneous, analogous measurements of polar NMs during the BR 2499 (2016 October 6 - 2016 November 1). The passage of a near-Earth ICME is indicated by vertical dashed lines (http://www.srl.caltech.edu/ACE/ASC/DATA/level3/icmetable2.htm).

Table 4 *(continued)*

Date	Onset	Duration	Dip/Peak	Amplitude	Interplanetary structure
	Time	Days		%	
2016 April 23	1.13 UT	1.16	PEAK	3.0	MB

Table 4 continued on next page

Figure 13. Same as Figure 13 for the BR 2492 (2016 March 31 - 2016 April 26).

Table 4 *(continued)*

Date	Onset Time	Duration Days	Dip/Peak	Amplitude %	Interplanetary structure
2016 June 16	0.15 UT	1.74	PEAK	2.5	MB
2016 June 21	23.11 UT	1.68	DIP	2.5	HCSC
2016 June 23	2.12 UT	1.95	DIP	2.5	CIR

Table 4 continued on next page

Table 4 *(continued)*

Date	Onset Time	Duration Days	Dip/Peak	Amplitude %	Interplanetary structure
2016 June 25	6.55 UT	1.79	DIP	2.5	CHSS
2016 June 30	7.19 UT	1.79	DIP	2.8	HCSC
2016 July 2	3.15 UT	2.00	DIP	2.8	MFE
2016 July 4	8.57 UT	1.74	DIP	2.5	CHSS+HCSC
2016 August 9	00.30 UT	0.75	PEAK	4.4	MB
2016 August 16	6.06 UT	1.79	DIP	2.5	HCSC
2016 September 15	22.43 UT	0.84	DIP	3.1	MFE
2016 October 11	13.25 UT	0.95	DIP	2.5	CHSS
2016 October 23	21.09 UT	0.95	DIP	3.8	HCSC+CHSS
2016 November 10	17.29 UT	1.16	DIP	3.8	CIR+HCSC
2017 January 14	12.52 UT	0.75	DIP	3.1	HCSC
2017 March 22	22.21 UT	1.05	PEAK	2.1	MB
2017 May 5	12.17 UT	1.46	DIP	2.3	MFE
2017 May 29	21.07 UT	1.53	DIP	2.4	CIR

7. CONCLUSIONS

A PD aboard LPF allowed for the measurement of the integral flux variation of GCR protons and helium nuclei above 70 MeV n^{-1}. The energy-dependence of FDs measured aboard LPF was compared to that of other space experiments and NMs which allow for a direct measurements of the integral flux variation of GCRs above effective energies > 10 GeV. A parameterization of pre-decrease energy spectra and energy spectra measured during the main phase of FDs is found to apply to different intensity events.

FDs observed in L1 are not correlated with geomagnetic storm occurrence unless the southward component (B_z) of the interplanetary magnetic field presents values < -20 nT. Finally, hourly averaged GCR flux variations measured with LPF allowed for the observations of non-recurrent features in the GCR integral flux variations > 0.75 days and < 2 days with intensities > 2%. These short-term depressions and peaks in the data trend appear correlated in the majority of cases with HCSC and plasma compression regions between subsequent CHSS, respectively.

REFERENCES

Adriani, O., Barbarino, G., Bazilevskaya, G.A., et al. 2011, ApJ, 742, 102

Aguilar, M., Alcaraz, J., Allaby, J., et al. 2002, PhR, 366, 331

Amaro-Seoane, P., Audley, H., Babak, S., et al. 2017, arXiv:1702.00786

Antonucci, F., Armano, M., Audley, H., et al. 2011, CQGra, 28, 094001

Antonucci, F., Armano, M., Audley, H., et al. 2012, CQGra, 29, 124014

Araújo, H. M., Wass, P., Shaul, D., Rochester, G., & Sumner, T.J. 2005, APh, 22, 451

Armano, M., Audley, H.,Auger, G., et al. 2016, PhRvL, 116, 231101

Armano, M., Audley, H.,Auger, G., et al. 2017, PhRvL, 118, 171101

Armano, M., Audley, H., Baird, J., et al. 2018a, ApJ, 854, 113

Armano, M., Audley, H., Baird, J., et al. 2018b PhRvL, 120, 061101

Armano, M., Audley, H., Baird, J., et al. 2018c APh, 98, 28

Armano, M., Audley, H., Baird, J., et al. 2018d PhRvD, 98, 062001

Badruddin, & Kumar, A. 2015, SoPh, 290, 1271

Barouch, E., & Burlaga, F. 1975, JGR, 80, 449

Beer, J. 2000, in Cosmic Rays and Earth, Space Science Review, ed. J. W. Bieber et al. (Amsterdam: Elsevier), 93

Benella, S., Grimani, C., Laurenza, M., & Consolini, G. 2019, NCimC, in press

Bones, C. W., & Simpson, J. A. 1976, ApJL, 210, L91

Burger, R. A., Potgieter, M. S., & Heber, B. 2000, JGR, 105, 27447

Cane, H. V. 2000, SSRv, 93, 55

Cane, H. V., Richardson, I. G., & von Rosenvinge, T. T. 1996, JGR, 101, 21561

Cañizares, P., Chmeissani, M., Conchillo, A., et al. 2011, CQGra, 28, 094004

Chauhan, M. L., Manjula, J., & Shivastava, S. K. 2011, ICRC (Beijing), 32, 261

Desai, M. I., Marsden, R. G., Sanderson, T. R., et al. 1998, JGRA, 103, 2003

Dremukhina, L. A., Levitin, A. E., Rudneva, N. M., & Gromova, L. I. 2011, in Physics of Auroral Phenomena, Proc. XXXIII Ann. Seminar, 55, http://pgia.ru:81/seminar/archive/2010/2_fields/02-01_Dremukhina.pdf

Forbush, S. E. 1937, PhRv, 51, 1108

Forbush, S. E. 1954, JGR, 59, 525

Forbush, S. E. 1958, JGR, 63, 651

Giacalone, J., Jokipii, J. R., & Kóta, J. 2002, ApJ, 573, 845

Gil, A., Asvestari, E., Kovaltsov, G.A., & Usoskin, I. 2017, Proc. ICRC (Busan), 35, 032, https://pos.sissa.it/301/032/pdf

Gleeson, L. J., & Axford, W. I. 1968, ApJ, 154, 1011

Gonzales, W. D., Jocelyn, J. A., Kamide, Y., et al., 1994, JGR, 99, 5771

Grimani, C., Araújo, H. M., Fabi, M., et al. 2011, CQGra, 28, 094005

Grimani, C., Benella, S., Fabi, M., Finetti, N., & Telloni, D. 2017, JPhCS, 840, 012037

Grimani, C., Fabi, M., Lobo, A., Mateos, I., & Telloni, D. 2015, CQGra, 32, 035001

Grimani, C., Vocca, H., Bagni, G., et al. 2005, CQGra, 22, S327

Hofer, M. Y., & Flückiger, E. O. 2000, JGR, 105, 23

Kane, R. P. 2010, AnGeo, 28, 479

Kim, R. S., Moon, Y.-J., Gopalswamy, N., Park, Y.-D., & Kim, Y.-H. 2014, SpWea, 12,246

Laurenza, M., Consolini, G., Storini, M., & Damiani, A. 2015, JPhCS, 632, 012066

Laurenza, M., Vecchio, A., Storini, M., & Carbone, V. 2014, ApJ, 781, 71

Lockwood, J. A. 1971, SSRv, 12, 658

Mateos, I., Diaz-Aguiló, M., Gibert, F., et al. 2012, JPhCS, 363, 012050

Mc Donald, F. B., Teegarden, B.J., Trainor, J. H., von Rosenvinge, T. T., & Weber, W. R. 1975, ApJL, 203, L149

Munini, R., Boezio, M., Bruno, A., et al. 2018, ApJ, 853, 76

Papini, P., Grimani, C., & Stephens, A. S. 1996, NCimC, 19, 367

Potgieter, M. S. 2013, LRSP, 10, 3

Richardson, I. G. 2004, SSRv, 111, 267

Richardson, I. G., Wibberenz, G., & Cane, H. V. 1996, JGR, 101, 13483

Sabbah, I. 2000, GeoRL, 27, 1823

Sabbah, I. 2007, SoPh, 245, 207

Sabbah, I., & Kudela, K. 2011, JGR, 116, A04103

Shaul, D. N. A., Aplin, K. L., Araújo, H., et al. 2006, in AIP Conf. Proc., 873, Laser Interferometer Space Antenna, ed. S. M. Merkovitz & J. C. Livas (Melville, NY: AIP), 172

Shikaze, Y., Haino, S., Abe, K., et al. 2007, APh, 28, 154

Stone, E. C., Frandsen, A. M., Mewaldt, R. A., et al. 1998, SSRv, 86, 1

Tsurutani, B. T., Burton, M. E., Smith, E. J., & Jones, D. E. 1985, Planet. Space Sci., 35, 289

Usoskin, I. G., Bazilevskaya, G., & Kovaltsov G. A. 2011, JGR, 116, A02104

Usoskin, I. G., Bazilevskaya, G., & Kovaltsov, G. A. 2017, JGRA, 122, 3875

Usoskin, I. G., Braun, I., Gladysheva, O. G., et al. 2008, JGR, 113, A07102

Usoskin, I. G., Kovaltsov, G. A., Adriani, O., et al. 2015, AdSpR, 55, 2940

Wass, P. J., Araújo, H. M., Shaul, D. N. A., & Sumner, T. J., 2005, CQGra, 22, S311

https://cdaweb.sci.gsfc.nasa.gov/index.html

http://www.srl.caltech.edu/ACE/ASC/DATA/ level3/icmetable2.htm

http://cosmicrays.oulu.fi/phi/Phi_mon.txt

www.nmdb.eu